Final Report

Project Name: Hanford Site-Wide Probabilistic Seismic Hazard Analysis (PSHA): High-Resolution Seismicity Analysis of the Yakima Fold and Thrust Belt Region, Washington

Contract Number: Battelle - 209054

Prepared by: Dr. Felix Waldhauser
423 W 120th Street, Apt 88
New York, NY 10027
Tel: 212 678 4804
Email: felixw@ldeo.columbia.edu

Prepared for: Pacific Northwest National Laboratory

January 31, 2014

Final Report

Hanford Site-Wide Probabilistic Seismic Hazard Analysis (PSHA):
High-Resolution Seismicity Analysis of the Yakima Fold and Thrust Belt Region, Washington

Battelle Contract 209054

Felix Waldhauser

January 31, 2014

1 Project objectives and overview of work performed

This project supports the Hanford site-wide Probabilistic Seismic Hazard Analysis (PSHA) project in the area of high-resolution seismicity analysis. Specifically, the focus of this project is to compute and analyze high-precision hypocenter locations for earthquakes recorded by the Pacific Northwest Seismic Network (PNSN) in the Yakima fold and thrust belt (YFTB) region in eastern Washington, between 121.25°W - 117.5°W and 46°N - 47.5°N (Figure 1), using the double-difference earthquake relocation method of Waldhauser and Ellsworth, 2000 together with phase arrival time picks from the Pacific Northwest Seismic Network (PNSN). The goal of this analysis is to improve the resolution in current earthquake catalogs in order to better image and characterize active faulting at seismogenic depths across the study region in support of the PSHA analysis.

The work performed during the project's duration (July 1 – December 31, 2013) can be divided into four main tasks:

1. Reformatting and quality check of PNSN P- and S-wave arrival time data (obtained from Alan Rohay) for 7667 earthquakes, focal mechanism data (file obtained from Jeff Unruh), and mapped surface fault data.
2. High-precision relocation of the seismicity in the YFTB study area using the HypoDD algorithm together with a suit of 1D and 3D velocity models, including determination of optimal weighting and inversion parameters and estimates of location uncertainties.
3. Evaluation and analysis of a final set of 5716 high-precision hypocenter locations and associated bootstrap error estimates for the YFTB study area, including investigation of discrepancy between locations obtain in this project and those obtained by Cliff Thurber.

4. Combined analysis of relocated seismicity, fault information, and focal mechanisms, focusing on the Wooded Island, Umtanum Ridge and Saddle Mountain regions. Comparison with previously published results.

This project is accompanied by the following deliverables that are all accessible at http://www.ldeo.columbia.edu/~felixw/Hanford/:

- Document (this report) that describes data and methods used, presents and discusses results and findings, and makes recommendations for future work.
- ASCII file including a catalog 5716 high-precision hypocenter locations and associated error estimates, with a file header describing data and format.
- Original data files on which this analysis is based on.
- Web-based tools that allow for 3D interactive viewing of the relocated seismicity.

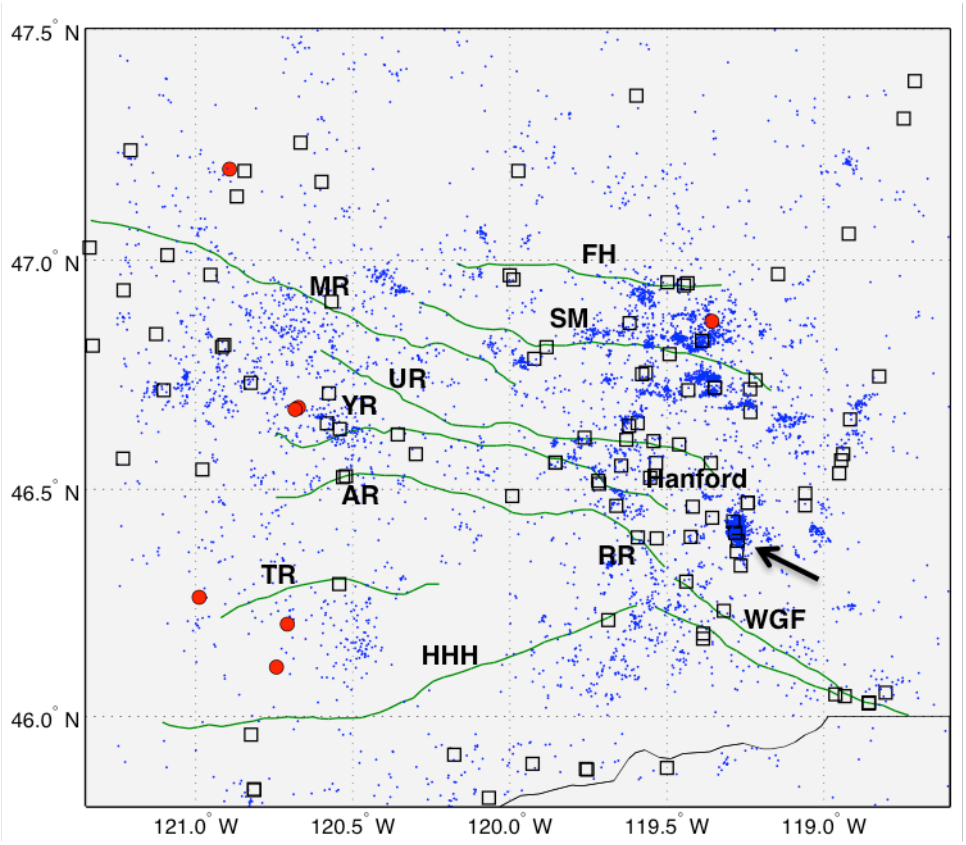

Figure 1 Overview of study area showing 7667 epicenters of earthquakes between 1969-2011 at their PNSN locations (blue dots; red dots are events M≥4), station locations (open squares), and quaternary faults (green lines). AR, Ahtanum Ridge; CH, Columbia Hills; FH, Frenchman Hills; ; HHH, Horse Heaven Hills; MR, Manstas Ridge; RR, Rattlesnake Mountain; SM, Saddle Mountains; TR, Toppenish Ridge; UR, Umtanum Ridge; WGF, Wallula Gap; YR, Yakima Ridge. Black arrow points to 2009 Wooded Island earthquake swarm.

2 Data and methods

The seismicity in the YFTB region is located in an area covered by the Columbia River flood basalts and can be broadly grouped into three categories: shallow (< ~2 km) events that occur in swarms, concentrated both temporally and spatially (Malone et al., 1975; Wickes et al., 2011; Gomberg et al., 2012), events that occur along crustal scale, mature faults (Blakely et al., 2011; Gomberg et al., 2012), and deep events (~14 – 20 km) that may be associated with a buried continental rift and possible associated fault zones (Johnson, 1989). Recent studies by Blakely et al (2011) and Gomberg et al (2012) provide a general description of the YFTB seismic activity and use the seismicity together with other geophysical data to gain insights on tectonic connections between forearc and back-arc regions of the Cascadia convergent margin (see also Johnson, 1989).

The data used for this project are 92,361 P- and 31,467 S-wave arrival time picks and hypocentral parameter estimates for 7,667 earthquakes recorded by the Pacific Northwest Seismic Network (PNSN) between 1969 and 2011 (Alan Rohay, pers. comm.; Figure 1). A total of 391 stations recorded the events that reach magnitudes up to M4.4. I did not use recordings from explosions because of their shallow locations and their limited ability to constrain the relative location of earthquakes. However, explosion data were used by Cliff Thurber to compute the 3D velocity model that I later use to predict the delay times in the double-difference inversion for event location.

Earthquake epicenters as estimated by the PNSN are rather sparsely distributed throughout the study region with a few clusters locating near mapped faults of the TFTB system (Figure 1). About 1,930 events (25%) of the total seismicity in the study region are included in a seismic swarm that started on January 4, 2009 in the area of Wooded Island (Wicks et al., 2011). The swarm earthquakes, ignoring events with fixed depths, are all shallow (< 2 km), with the largest event having a magnitude M=3.7.

I used the double-difference earthquake algorithm *HypoDD* (Waldhauser and Ellsworth, 2000; Waldhauser, 2001) to relocate the earthquakes. The double-difference method minimizes, in a weighted least squares sense, residuals between observed and predicted travel time differences for pairs of earthquakes to solve for adjustments in the vectors connecting the hypocenters through the partial derivatives of the travel times for each event with respect to the unknown. With this approach common mode travel time errors are minimized, leading to significant improvement in the resolution of routinely produced catalogs of earthquake locations (for details see Waldhauser and Ellsworth, 2000). The *HypoDD* algorithm is used worldwide for analyzing seismicity at various scales to address a wide range of seismological and seismotectonic problems. For this project I used *HypoDD* version 2.1b (January 2013), which includes 3D ray-tracing capability (using a variation of Um and Thurber's bending method) that was first implemented and tested in Rietbrock and Waldhauser (2004). I used the conjugate gradient method (LSQR) to solve the system of double-difference equations, and for comparison I estimated locations and formal errors for subset of events via singular value decomposition (SVD).

My double-difference analysis is based on the full PNSN data set. Note that I have not preselected the original data based on parameters such as solution quality or RMS values. The HypoDD weighting functions are best suited to sort out the good from the bad. The only a-priori requirement for events to enter the double-difference process is that they were recorded on at least 5 stations (6 for the Wooded Island swarm). I

performed a series of initial relocation runs to find optimal double-difference parameters to relocate the entire study region as comprehensively as possible, and at the same time aim for highest resolution in areas of high event density or station coverage such as the Wooded Island swarm. While the Wooded Island swarm events are generally well recorded by nearby well-distributed stations and linked over very short distances (~1km), this is not necessarily the case for the rest of the seismicity. This situation requires different parameters for computing the differential time network and the relocations. I borrowed some concepts and tools from our comprehensive, regional-scale relocation work in northern California (Waldhauser and Schaff, 2008) in order to optimize the resolution in the double-difference locations across our study area.

I initially used as starting locations the locations from the 7667 events in the PNSN catalog and then updated the PNSN catalog with Cliff Thurber's 3D located solutions (4605 event) after they became available (file hanford.reloc_sm05FW). I removed the absolute location bias in the PNSN locations, as revealed by the 3D located events, by relocating each event in the PNSN catalog relative to a nearby 3D located event using a single-event double-difference algorithm (Waldhauser, 2009). This procedure uses the absolute location information from the 4605 3D located events to remove the absolute location bias for the rest of the events in the original PNSN event file. I updated the original PNSN phase file with the improved hypocentral information for all events and used it as the new basis for the final analysis, including the rebuilding of the differential time network.

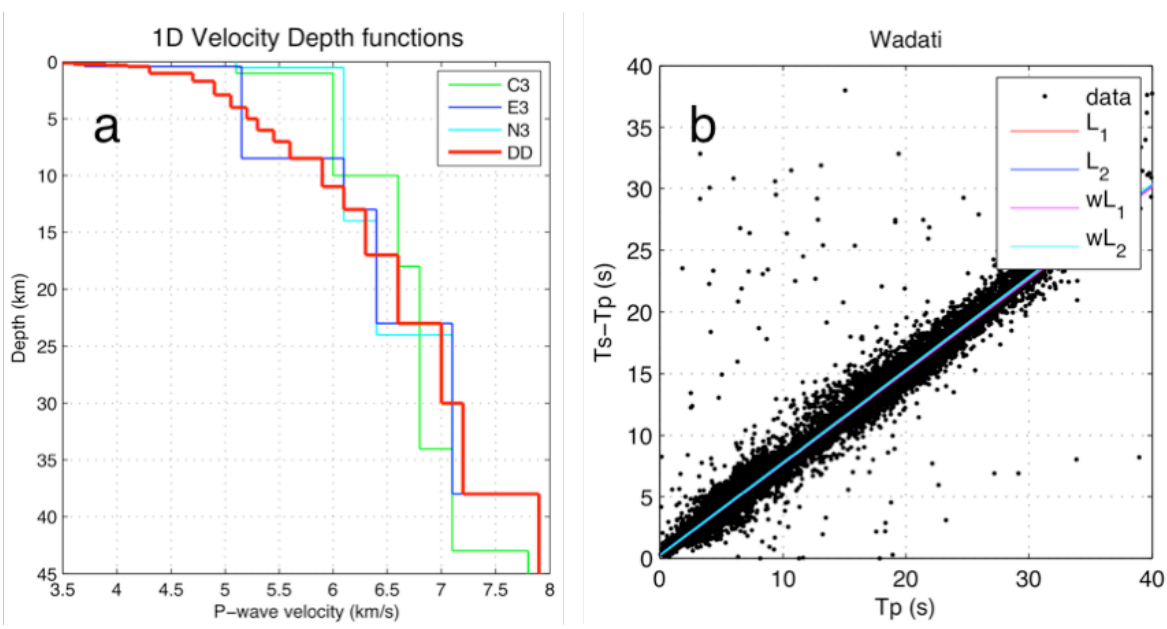

Figure 2 a) Layered, depth-dependent 1D velocity models used for routine location at the PNSN (C3, E3, N3) and a re-sampled E3 based model used in this project for double-difference relocation. b) Wadati diagram showing regular and weighted L1 and L2 norm fits to all travel time data. The slopes of the fitted lines yield a vp/vs ratio of 1.75 for both the Wooded Island area and for the entire study area excluding the Wooded Island area.

I tested several models for predicting the delay times and ray parameters in the linearized inversion of the HypoDD procedure. I ended up using two models for the final analysis; the first model is a re-sampled version of the 1D P-velocity depth function E3 used for routine location at the PNSN in the region (Alan Rohay, pers. comm.; Figure 2a). Notable differences between models from adjacent regions (C3 and N3) and model E3 are the slower velocities of model E3 in the top 10 km of the crust. I performed a Wadati analysis of the P- and S-arrival times to estimate a Vp/Vs ratio of 1.75 (Figure 2b), which I used to scale the P-velocity values of re-sampled model E-3 to obtain the 1D S-velocity values. The Vp/Vs ratio appears to be relatively robust across the study region. The Wadati plot reveals only a small number of outliers, indicative of consistently picked arrival times. The second model is the 3D tomographic model from Cliff Thurber (file Vps_model_sm05FW.dat), which he also used to compute the improved absolute locations.

3 Relocation results

From the original 7667 events in the original PNSN catalog I was able to relocate 5930 events with the 1D model and 5716 events (HypoDD-1D) with the 3D model (HypoDD-3D) (Figure 3). The differences between the original PNSN (Figure 1) and the relocated HypoDD locations have means (standard deviations) of 0.27 km (1.2 km) and 0.6 km (2.6 km) in horizontal and vertical directions, respectively. These values are comparable to differences we obtain from our relocation work in Northern California (Waldhauser and Schaff, 2008). The most notable difference is the correction of the fixed near-surface depths in the PNSN catalog (Figure 4), dominated by events in the Wooded Island swarm. Figure 5 shows a comparison between original PNSN locations and corresponding HypoDD-1D relocations for Wooded Island swarm events. The DD relocations reveal detailed faults structures that were previously hidden in the uncertainty and unresolved depth estimates of the PNSN locations (see Section 4.1).

A comparison between the 1D and 3D HypoDD solutions indicates relatively small location differences; average differences (standard deviations) are 0.04 km (0.5 km) horizontally, and 0.05 km (1.1 km) vertically. It appears that event depths obtained in the 3D model are somewhat shallower than those obtained in the 1D model, with most of that shift occurring in the Wooded Island region (Figure 4) (see Section 4). Both 1D and 3D HypoDD relocations sharpen the seismicity in most areas across the study region. They resolve active structural features at seismogenic depths that were previously hidden in the location uncertainty of the PNSN data, in particular in the Wooded Island, Umtanum Ridge, and Saddle Moutain region. A detailed analysis of the seismicity, using the 3D model based HypoDD solutions, together with focal mechanisms and mapped fault traces is given in Section 4.

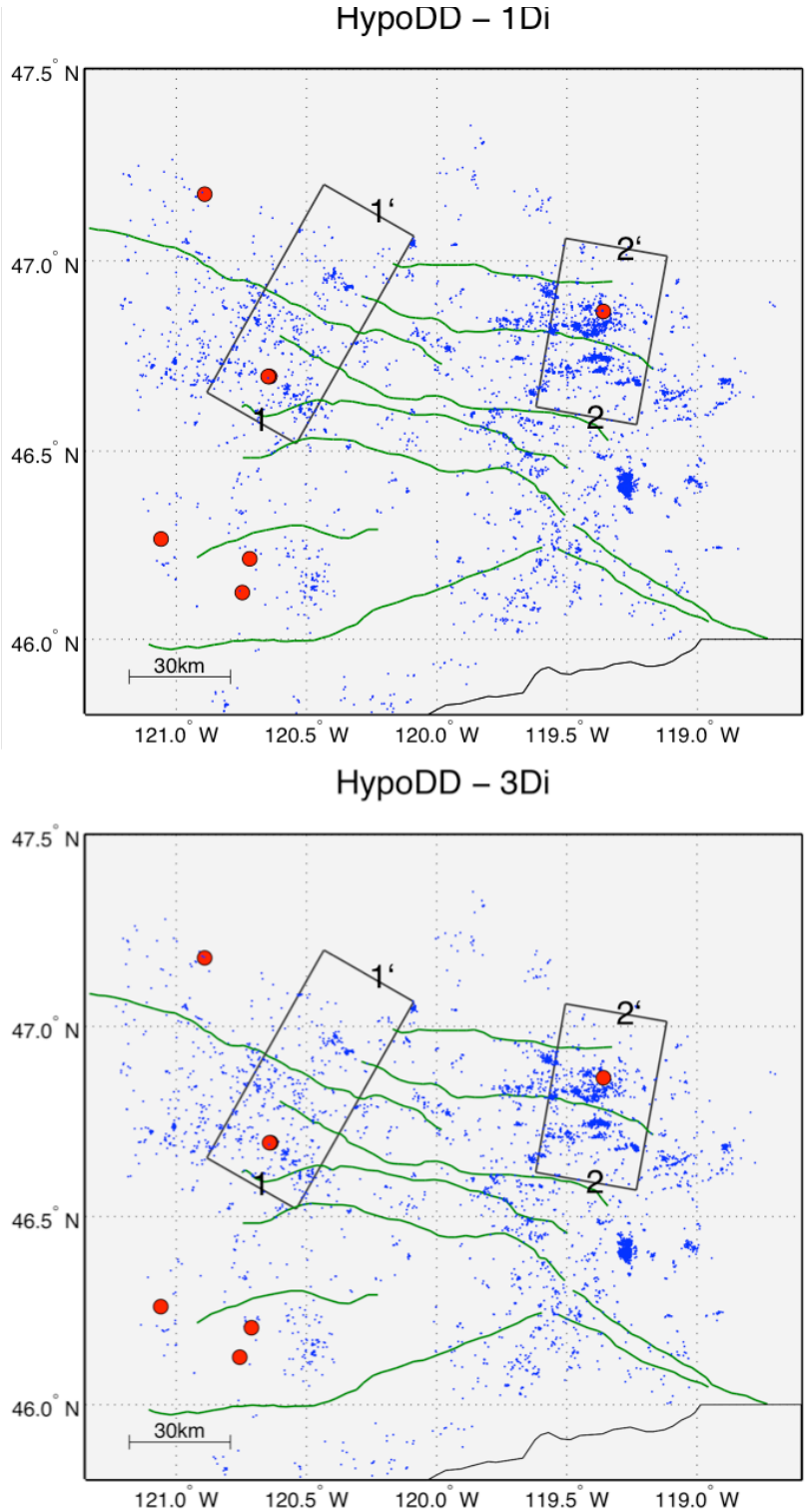

Figure 3 HypoDD relocations of 5,930 events computed with the 1D model (top panel) and 5,716 events computed with the 3D model (bottom panel). Blue dots are event epicenters, red dots denote events with M≥4, green lines faults. Annotated boxes in lower panel include events shown in Figure 10 and Figure 11. The earthquake locations shown here can be viewed in 3D at http://www.ldeo.columbia.edu/~felixw/Hanford/YFTB.3d.html

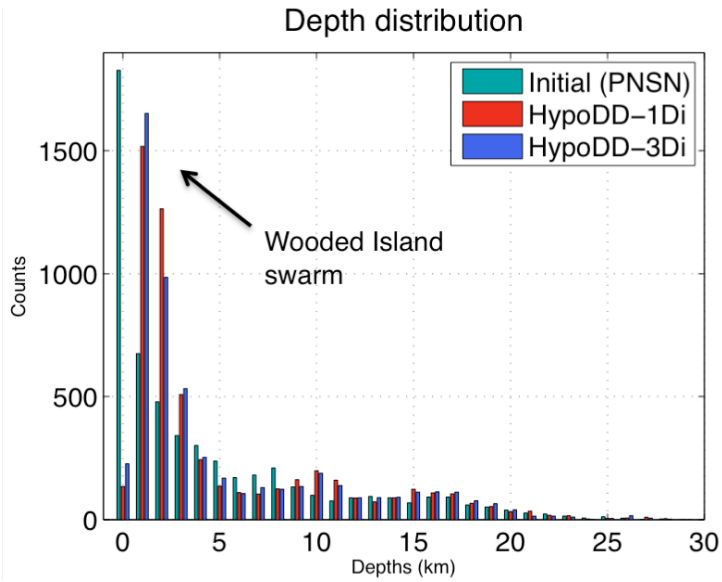

Figure 4 Distributions of initial (PNSN) depth estimates and depths from HypoDD 1D and 3D inversions.

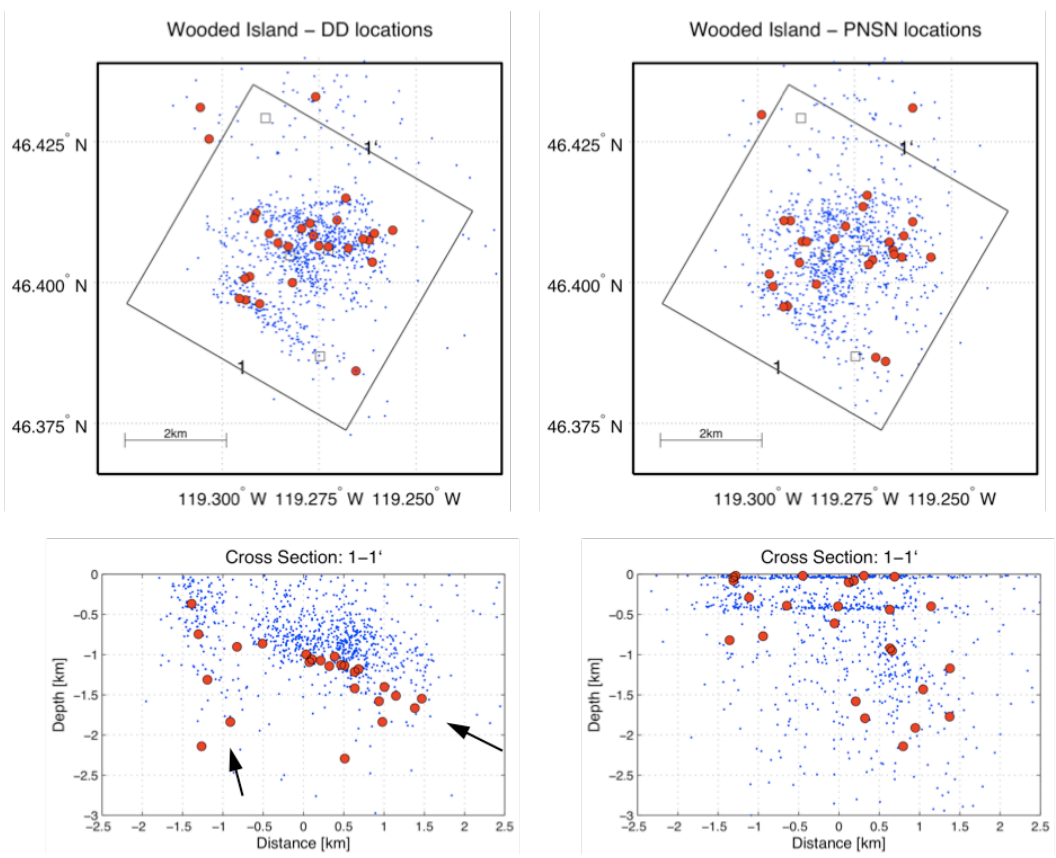

Figure 5 Map view (top panels) and cross-section(lower panels) of 1,357 HypoDD-1D locations of events included in the Wooded Island swarm (left panels). Corresponding PNSN locations are shown for comparison (right panels). Red dots denote events with M≥2.5. Open squares in map views are station locations. Arrows point to inferred faults. Box in map view includes events shown in cross section (lower panel).

3.1 Residuals and location error estimates

The residuals RMS values for the entire region are 0.093 s for the 1D, and 0.083 s for the 3D case (Figure 6a), consistent with the expected pick accuracy of the arrival time data. They are much smaller (0.008 s) for the Wooded Island region where station and event distribution are dense. The initial residuals are 0.3 s for the entire region and 0.1 s for Wooded Island.

To compute relative location errors I bootstrapped and relocated the final double-difference residual vector 200 times and computed the horizontal and vertical projection of the 95% confidence ellipses from the sample distribution (Figure 6b). Most of these uncertainties range from a few to several tens of meters, with depths typically more poorly constrained than the horizontal locations. Absolute location uncertainties may be larger, but less than 1 km on average, based on the variance in solutions from various HypoDD runs with 1D and 3D models, and comparison between solutions based on1D and 3D located starting locations.

I ran several tests to evaluate the robustness of the final double-difference locations. In one of them I introduced bias in the starting absolute locations for some well-constrained Wooded Island events. I relaxed the numerical constrain on the centroid shift in HypoDD, and relocated the events allowing for shifts in the cluster centroid (see Waldhauser and Ellsworth, 2000 for details). The results showed that the delay time data provide sufficient constraint for HypoDD to resolve the absolute locations too, removing the absolute location bias in the relocated earthquakes.

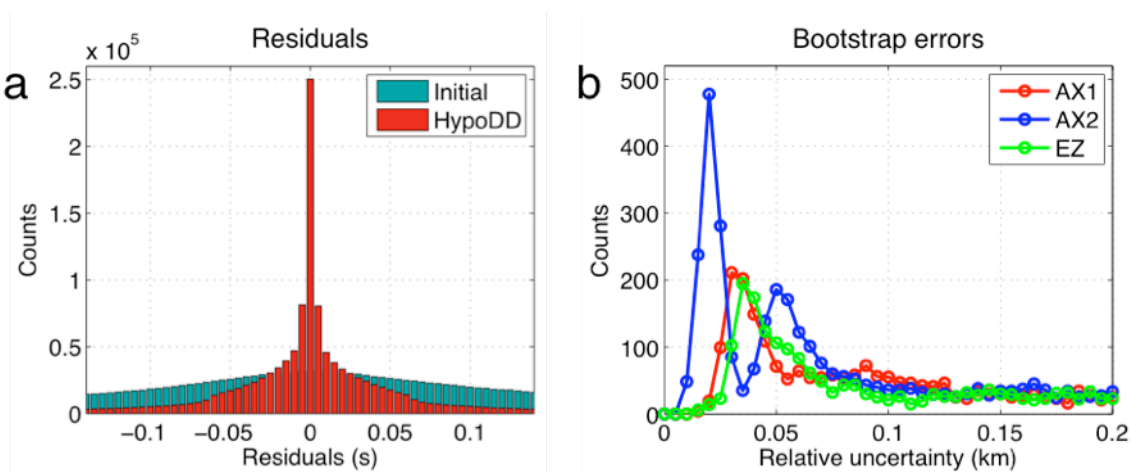

Figure 6 a) Distribution of initial and HypoDD.3Di double-difference residuals for the entire study region, and b) relative location errors from bootstrapping shown as major (AX1) and minor (AX2) axis of the horizontal and vertical (EZ) projection of the 95% confidence ellipses.

3.2 Some comparisons with locations from Cliff Thurber

I have performed a comparison between my HypoDD catalog (5716 events) and Cliff Thurber's tomoDD locations as listed in his file reloc.sm05FW (4605 events). Note that I used the locations in this file as starting location in HypoDD. There were some differences between the corresponding events in the two catalogs. The standard deviations were 0.9 km in E-W, 0.7 km in N-S, and 1.5 km in vertical direction (Figure 7). A significant difference existed for the absolute depth of the Wooded Island swarm (Figure 8a,b). The HypoDD-3D solutions were about 0.4-0.5 km shallower than the corresponding tomoDD locations. I did the following checks:

- I tested several double-difference parameters, but I could not find a combination that pulls events up by almost half a km.
- I performed a test where HypoDD successfully restored the absolute locations after applying significant shifts to the centroid of the initial locations, indicating that the differential time data can resolve bias in absolute locations in this region.
- The HypoDD-1D solutions were somewhat deeper than the HypoDD-3D locations, but still shallower than the tomoDD solutions, suggesting that the vertical shift in the HypoDD-3D solutions had something to do with the 3D model. I ruled out that the problem is with the correct orientation and positioning of the 3D model (the model Cliff gave me was a left handed system, but what I needed for HypoDD is a right handed orientation).
- Finally, there is a significant difference between the Vp/Vs ratio in Cliff Thurber's tomographic model for the Wooded Island area and the Vp/Vs ratio determined from the Wadati analysis (Figure 2b). The swarm is in a cell of the tomography model that ha a P-velocity of about 3.5 km/s, but very low vp/vs ratio (1.4). The Wadati analysis however indicates a Vp/Vs of 1.75. Runs with several 1D models and a range of Vp/Vs ratios can explain some of the shift, but not all.

Hypocenters in Cliff's latest relocation file (reloc_sm10FW3s.txt), however, are shallower in the Wooded Island region, and more consistent with, but still 200 m deeper than the HypoDD locations (Figure 8c). The location differences between the two tomoDD files have standard deviations of 1.3km (E-W), 1.1km (N-S), and 2.3 km (depth), and means of -0.1 km (E-W), -0.04 km (N-S), and 0.14 km (depth).

All catalogs reveal the first order structure of seismicity discussed in my first progress report. Specifically, from the location of the larger events in the swarm (M≥2.5; red dots in Figure 8) we can infer a ~45° NE dipping fault between 0.7 and 2 km depth. The fault appears to cut off diffuse seismicity in the hanging wall. The cutoff as defined by larger events is especially well imaged in the HypoDD locations. To the SW of the seismogenic 'wedge' the relocated seismicity indicates a steeply NE dipping fault from the surface down to ~2 km.

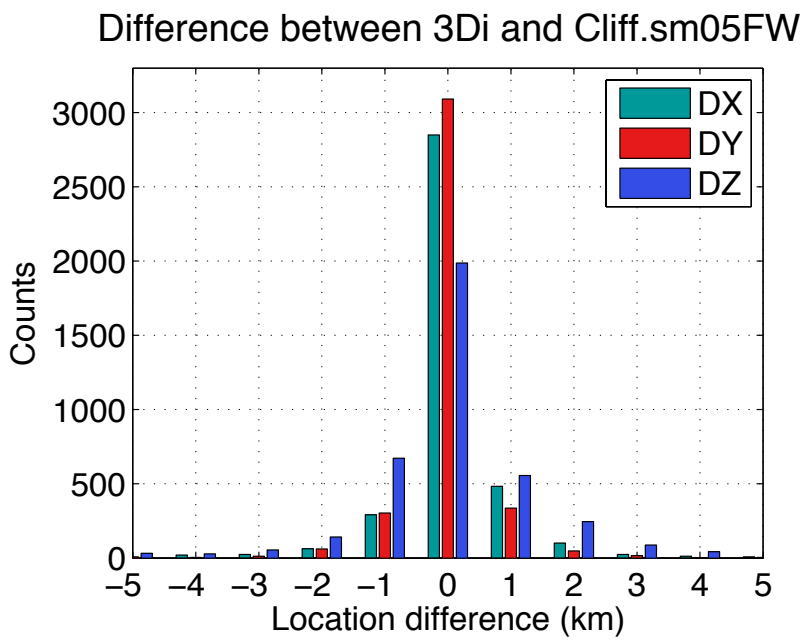

Figure 7 Difference between the HypoDD locations (3Di) and corresponding locations in Cliff Thurber's file reloc.sm05FW.

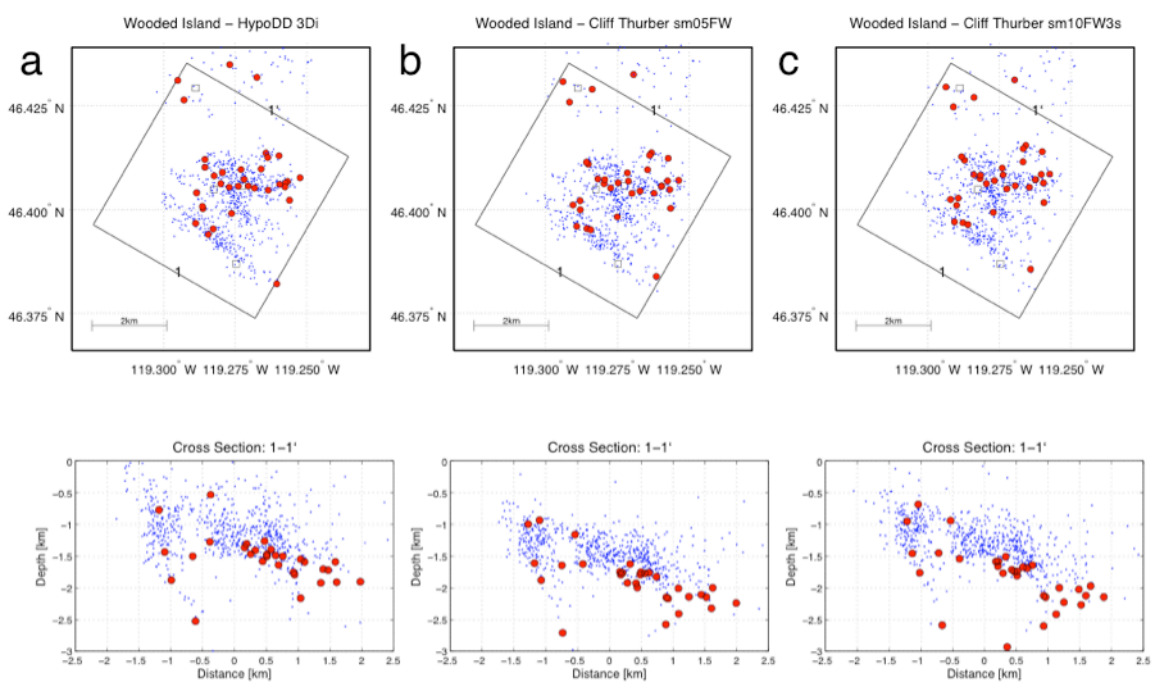

Figure 8 Comparison (top: map view; bottom: cross sections) between 789 corresponding events in the Wooded Island swarm from my final HypoDD-3D catalog (a) and two version of Cliff Thurber's catalog: sm05FW (b) and sm10FW3s (c). Red dots are events with M≥2.5.

4 Relocated seismicity, focal mechanisms, and fault surface traces

In this section I am investigating the HypoDD relocated seismicity in combination with available focal mechanisms and geologic information for three regions: the Wooded Island area SE of Hanford which is the location of the 2009 seismic swarm (Malone et al., 1975; Wicks et al., 2011; Gomberg et al., 2012), the Umtanum Ridge (Blakely et al., 2011) and the Saddle Mountain regions. In particular, I am using the combined data sets to evaluate the consistency (or lack thereof) between structures seen in the seismicity and the kinematics of individual earthquakes, and their correlation with mapped faults at the surface (shown in subsequent figures as green lines in map views and green triangles in cross sections). This provides an independent check on the reliability of the new hypocenter data. I used the focal mechanisms listed in the file "focal.AMcards.aki" which I obtained from Jeff Unruh. They were computed from first motion polarities (using FPFIT?) and include mechanisms for events between 1970 and June 28, 2010. Note that I did not re-compute the mechanisms at the relocated hypocenter positions.

4.1 Wooded Island swarm

From the relocated seismicity, and especially from the location of the larger events in the swarm (M≥2.5; red dots in Figure 9), we can infer a NW striking, steeply NE dipping fault (W1) in the southwestern part of the swarm. In the northeastern part of the swarm the larger events appear to define a ~45° NE dipping fault between 0.7 and 2 km depth (W2). The fault appears to cut off diffuse seismicity in the hanging wall. The internal structure of this seismogenic 'wedge' defined by fault W2 seems to be more complicated than can be appreciated in a single cross-section as shown in Figure 9. When investigated with an interactive 3D viewer (http://www.ldeo.columbia.edu/~felixw/Hanford/Wooded_Island_swarm.3d.html), one can appreciate that the NE part of the swarm could also host at least two, possibly intersecting sub-faults (e.g., a NW striking, steeply dipping fault that is sub-parallel to the near-vertical fault W1, and a more westerly trending shallow dipping fault).

Focal mechanisms available for earthquakes in the Wooded Island Swarm (Figure 9) are quite diverse in nature, including reverse but also normal faulting events, some of the events with a significant oblique component. These mechanisms do not correlate well with what I believe are active faults (W1, W2) based on the seismicity. This may reflect true complexity, remaining uncertainty in the locations, uncertainty in the focal mechanisms, or a combination of all. Since the events represent swarm activity, much of the variation in focal mechanisms can likely be attributed to faulting complexity.

Although it is difficult to compare our relocation results with the relocation results of Wicks et al. (2011) due to the low resolution/small size of their Figure 5, their fault model (their Figure 7) based on their combined analysis of InSAR and earthquake data shows a ~45° NE dipping thrust fault that is consistent with my and Cliff Thurber's results in the NE part of the swarm (assuming that the few thrust mechanisms along W2 represent the dominant mode of failure). It is not clear, however, to what degree the near vertical fault W1 found in this study would change the InSAR modeling results. Given the lack of depth control when inverting surface deformation data, it is possible that the InSAR data would also fit a model where slip occurs on two faults as defined here or potentially more faults.

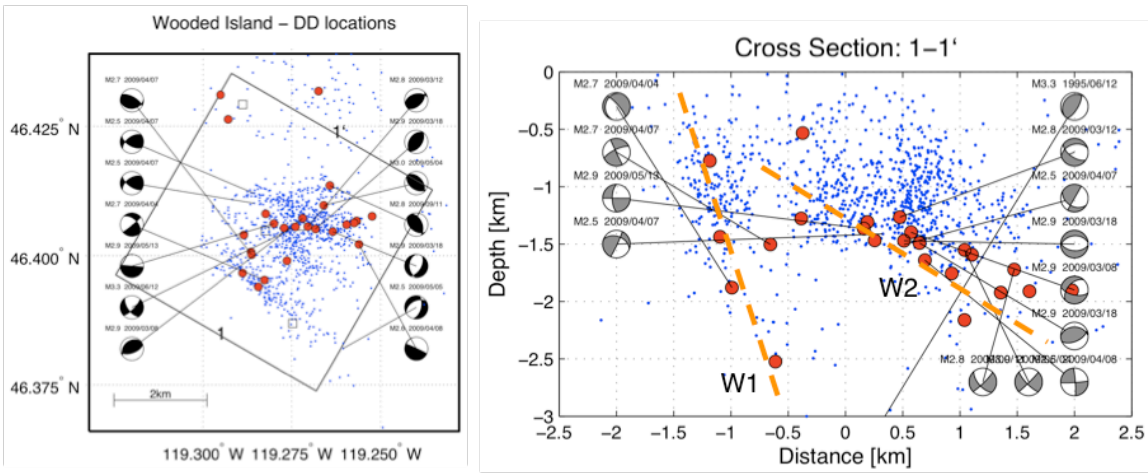

Figure 9 Map view (left) and cross section (right) of hypocenter locations (blue dots) and focal mechanisms for Wooded Island swarm events. Red dots are events with M≥2.5. Squares in map view are station locations. Box in map view includes events shown in cross section. Focal mechanisms are lower hemisphere projection in the map views, and side projections in the cross-sections. Box in map view includes events shown in cross section. Labeled, dashed orange lines denote inferred faults.

4.2 Umtanum Ridge

While in some cases the sparseness of the event distribution in the Umtanum Ridge region makes it difficult to see clear spatial trends in the seismicity, a closer look at the location of the larger events reveals some correlation between seismic activity, focal mechanisms, and active faults mapped at the surface in some areas.

Compared to the seismicity in Wooded Island area, hypocenters in the Umtanum region reach greater depths (<20 km), and focal mechanisms, mostly reverse in nature, are more consistent. In general, the focal mechanisms are consistent with the fault structures I identified in my previous reports along a profile crossing the Yakima Ridge (YR), Umtanum Ridge (UR), Manstas Ridge (MR), and the Saddle Mountain faults (SM) (Figure 10). The profile roughly coincides with a near surface structural profile presented in Blakely et al (2011) (Figure 10, bottom panel), but exact correlation between the fault traces used in this study (QUAKE-FAULT.9-30-01; shown as green lines and triangles in Figure 10) and the ones shown in the Blakely profile is not always clear. Blakely et al. (2011) develop the detailed upper crustal model shown in the lower panel of Figure 10 using gravity and magnetic data constrained by geologic mapping and three deep exploratory boreholes.

The most striking structural feature is seen in the cross section of Figure 10 at 12 km model distance, where the shallow events appear to activate the western extension of the Saddle Mountain fault to a depth of ~5 km, and possibly deeper. Many (but not all) of the focal mechanisms support the near-surface observations and interpretation by Blakely et al (2011), although direction of movement on the fault appears to be reversed.

The seismicity also supports a steeply southwest dipping fault (U2) down to about 20 km depth that appears to be related to Manstas Ridge fault (MR). However, many

focal mechanisms are not consistent with that interpretation (although some are), and it is possible that this portion of the profile is complicated by the interaction of the southwest dipping Manstas fault (U2) and (conjugate) northeastern dipping faults related to movement on the Umtanum Ridge fault (UR).

Finally, we can infer a reverse fault (U3) that correlates with the Yakima Ridge fault (YR) mapped at the surface. Although the relocated seismicity is quite sparse along the proposed fault between 0 and 10 km depth, the focal mechanisms are mostly consistent with it. The M4.3 earthquake of December 2, 1987 appears to have activated that fault. The seismicity as well as focal mechanisms along this portion of the fault again suggests that significant activity occurs on conjugate faults. It is important to note that, in generating the cross-section shown in the middle panel of Figure 10, I projected the hypocenters perpendicular to the direction of profile 1-1'. While such a projection seems to be appropriate for events associated with the NW trending Umtanum Ridge and the Manstas Ridge (MR) faults, this might not be the case for events along the Yakima ridge (YR). The Yakima Ridge fault seems to exhibit a general east-west trend near the surface (green lines in Figure 10), but it is not clear whether that trend is maintained at depth.

Alternative solutions to the ones outlined above may also be possible and need to be investigated in a more detailed geologic and tectonic context. A careful revisit of the focal mechanisms, in particular the computation of their solutions at the relocated positions, would likely help to better take advantage of the high spatial resolution of the seismicity that is now available.

4.3 Saddle Mountain

Relocation results from the Saddle Mountain region indicate that most earthquakes locate near the surface at depths shallower than 4 km (Figure 11). Obvious structural features revealed in my last report (S1-S4) are again highlighted in the cross sections of Figure 11. Of particular interest is a feature that can be correlated with the mapped Saddle Mountain fault (S1), and a north dipping reverse fault (S3) that hosts the M4.4 thrust event of December 20, 1973. One other clear feature (S2) in cross section 1-1' does not have a mapped surface expression. In cross section 2-2' I show a cluster of events that, in map view, seems to be associated with the Saddle Mountain fault. In cross section, however, the events align along a south dipping structure that has an apparent surface piercing point that lies about 4 km north of the mapped surface trace. Three focal mechanisms along the fault show normal fault mechanisms, one is of reverse type. This is in contrast to the proposed fault S1 to the east, which we infer to be north dipping and connecting to the mapped fault at the surface. It is possible that feature S4 is a conjugate fault, or that it is somehow related to the bend seen in the mapped Saddle Mountain fault in that particular area.

Some rather diffuse seismicity with a wide range of faulting styles exists in the depth range 12 to 18 km (red circle in Figure 11b). I don't see an obvious connection between the deep events and the shallow structures, although two focal mechanisms are consistent with a deep extension of the Saddle Mountain fault. It is possible (or likely) that the deep activity beneath the Saddle Mountain region is related a buried continental rift and possible associated fault zones (Johnson, 1989).

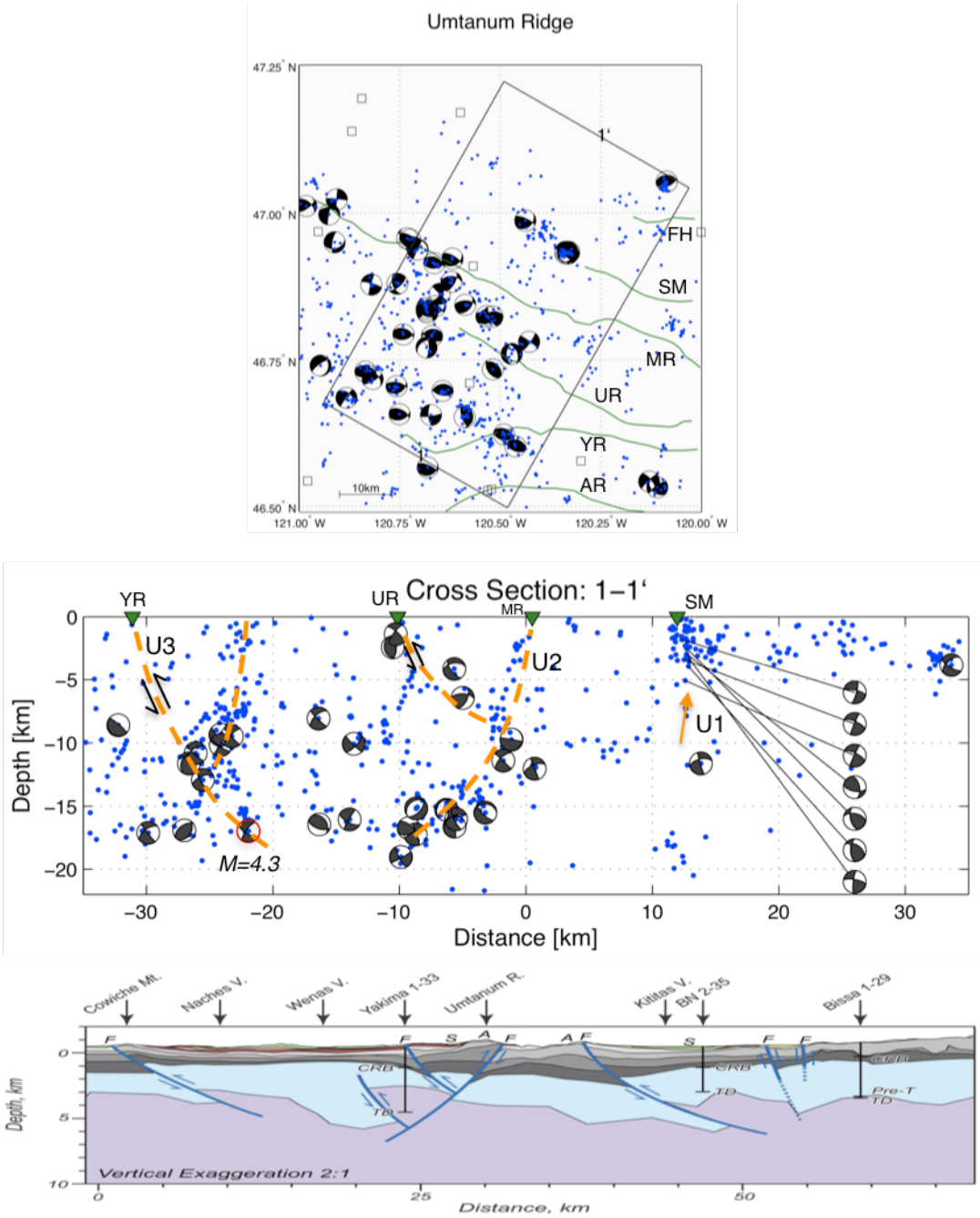

Figure 10 Map view (top panel) and cross sections (middle panel) of hypocenter locations (blue dots) and focal mechanisms for the Umtanum Ridge region. Squares in map view are station locations. Box in map view includes events shown in cross section. Labeled, dashed orange lines are proposed faults. Focal mechanisms are lower hemisphere projection in map view, and side projections in cross-section. Green lines in map view and green triangles in cross section are locations of mapped surface traces. Bottom panel: geologic/structural profile of Blakely et al. (2011). Note: No vertical exaggeration in this modified version. The two cross sections are aligned at approximately the same location (i.e., 0 km distance in Blakely profile is -34 km in seismicity cross section). However, the one to one correspondence of the location and naming of the fault traces is not clear.

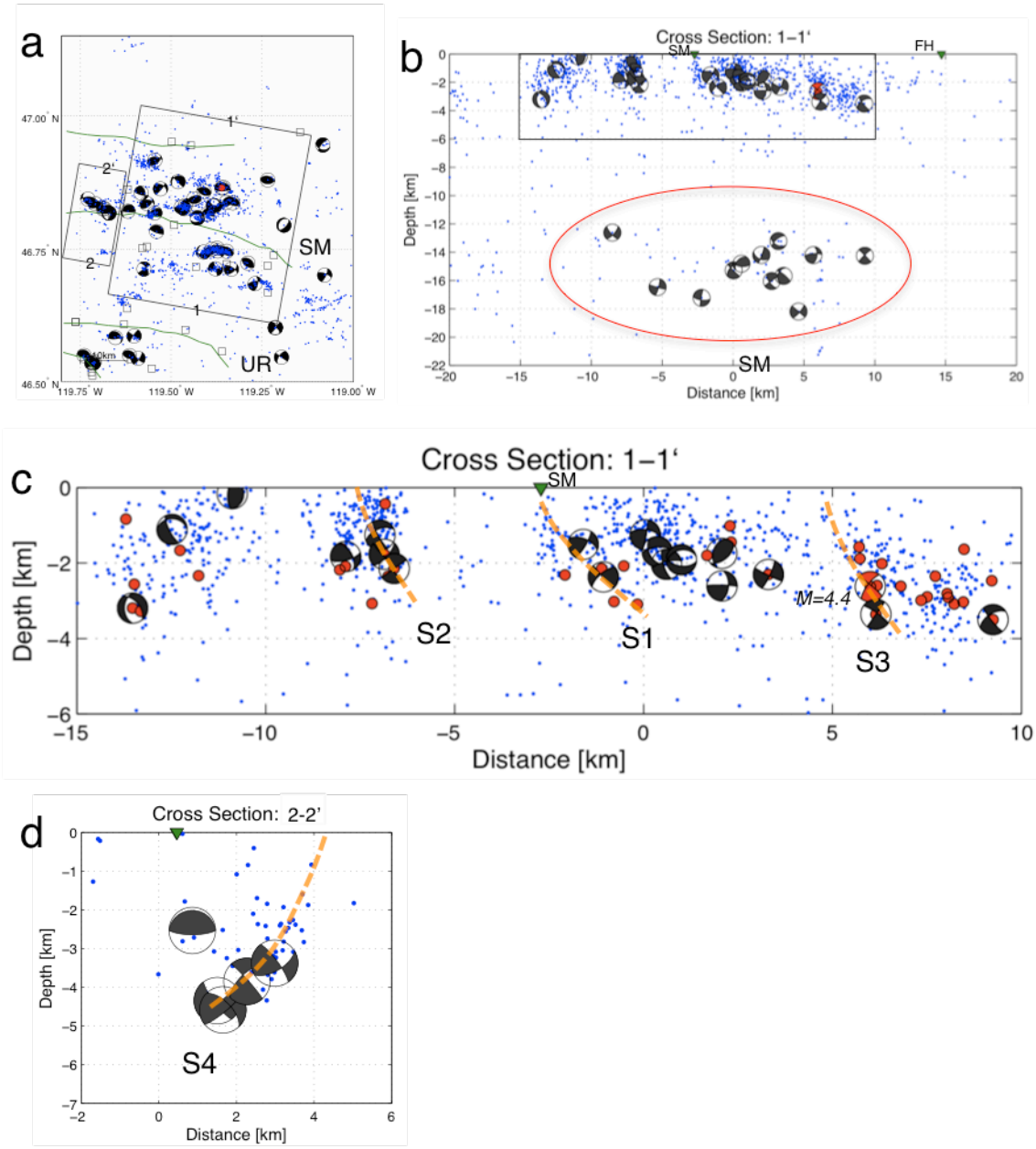

Figure 11 Map view (a) and cross sections (b-d) of hypocenter locations (blue dots) and focal mechanisms for Saddle Mountain region. Squares in map view are station locations. Green lines in map view and green triangles in cross section are locations of mapped surface traces. Annotated box in map view includes events shown in cross section. Box in b) includes events shown in c). Labeled, dashed orange lines are proposed faults. Focal mechanisms are lower hemisphere projection in map view, and side projections in cross-section. Red dots in cross sections are events with M≥2.5. Red focal mechanism denotes 1973 M4.4 event. Red circle points out deep events of diverse rupture mechanisms and no obvious association with structural features. FH = Frenchman Hills; SM= Saddle Mountain Fault.

5 Conclusions

This project produced high-precision double-difference hypocenter locations for the YFTB region that improve the resolution in existing PNSN locations. The HypoDD relocated seismicity resolves apparent active structural features at seismogenic depths that were previously hidden in the location uncertainty of the PNSN data. A detailed analysis of the relocated seismicity together with focal mechanisms and mapped fault traces is carried out for three seismically active regions: Wooded Island, Umtanum Ridge, and Saddle Mountain. In all three regions the analysis lead to an improved characterization of fault structures and kinematics and evaluation of their relationship to near surface information. The active faults imaged by the relocated seismicity are generally consistent with the local and regional tectonics, and previously published results.

The analysis also revealed discrepancies between seismicity, focal mechanism and near surface data in a couple of locations. Some of these discrepancies may be due to source complexities, structural complexities, or a combination of both. Others are likely due to inaccuracy in the data used, the methods employed, or combination of both. Some of the following suggested additional analysis may help address these issues, but there is no guarantee that they will.

1. Assessing the robustness and potentially improving the quality and resolution of available focal mechanisms by re-computing them at their improved (relocated) hypocenter position.
2. Improving the precision of the pick-based delay times, and thus relative event locations, by using waveform cross-correlation methods (e.g., Schaff et al., 2004). It is difficult to foresee the improvement in location precision by incorporating correlation data. High-quality manual picks as used in this study are typically good enough to resolve fault structures at the tens to hundred meters scale. Furthermore, nearby events in complex systems may not produce waveforms at common stations that are similar enough for precision delay time measurement. In Waldhauser and Schaff (2008) we compared network locations with pick-based and cross-correlation based relocations for four different tectonic regions in Northern California (Figure 12). I would judge the Northern California Seismic Network data as being similar in quality and consistency to the PNSN data used in this study. Note, however, that a thorough correlation analysis not only has the potential to improve location precision, it also provides critical information about source characteristics and fault properties, and may be used to find repeating earthquakes that may be useful in PSHA.
3. It is likely that the current double-difference locations can be further improved by relocating events across small areas with a dedicated focus on a particular fault or fault system. In the course of such specialized studies the robustness of the double-difference locations could be further tested with synthetic data and additional bootstrap and jackknife methods.

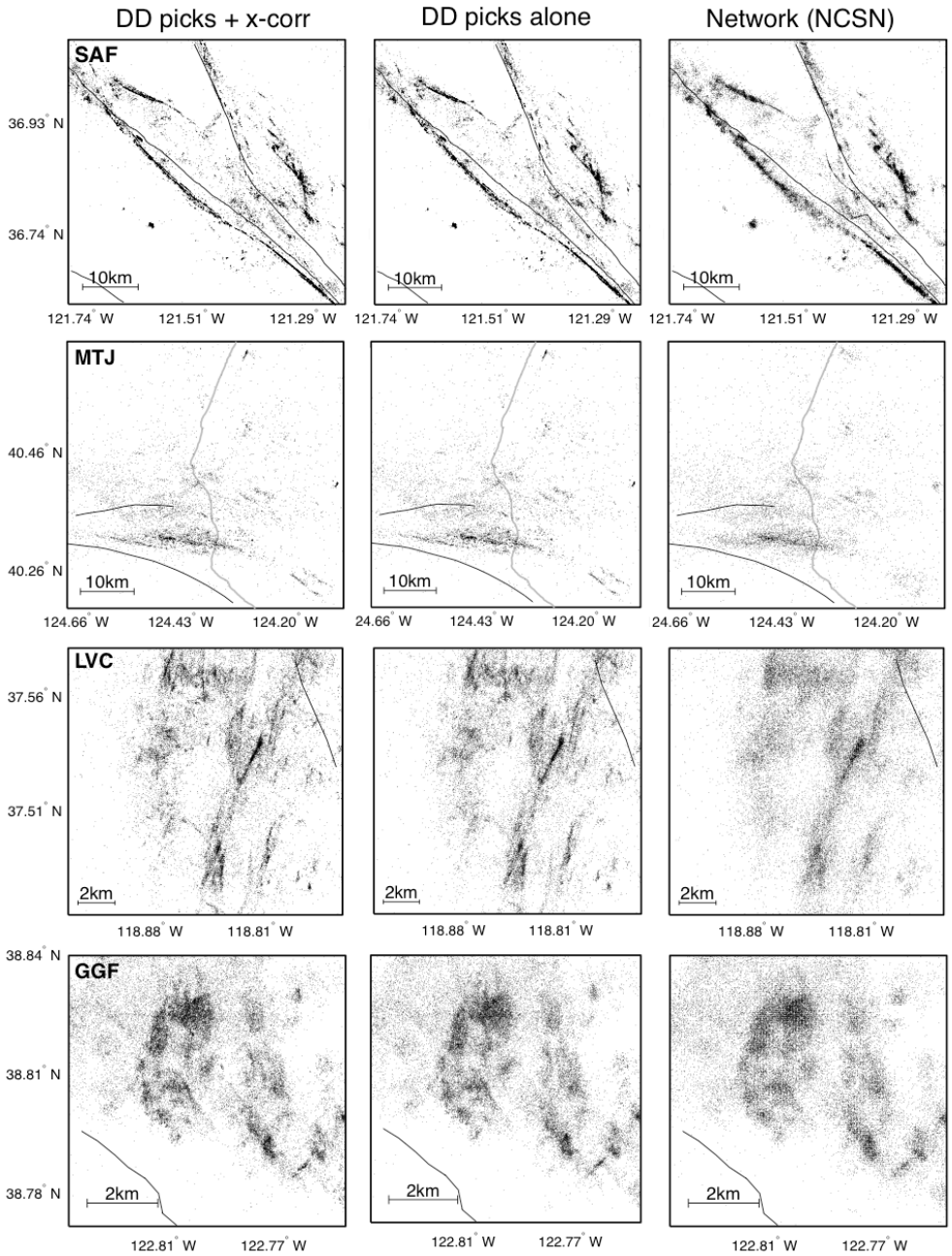

Figure 12 Comparison between cross-correlation (left panels) and pick-based (middle) double difference locations and network locations (right panels) for four different tectonic regions in Northern California. The same events are displayed in each of the three panels. SAF= San Andreas Fault; MTJ = Mendocino Triple Junction; LVC = Long Valley Caldera; GGF = Geysers Geothermal Field. Note the networks of discrete faults imaged in the relocated seismicity in the tectonic regions SAF, MTJ, and LVC, compared to sharpened ''clouds'' imaged in the region of induced seismicity at GGF. Lines indicate mapped surface fault traces. From Waldhauser and Schaff (2008).

References

Blakely, R. J., B. L. Sherrod, C. S. Weaver, R. E. Wells, A. C. Rohay, E. A. Barnett, and N. E. Knepprath (2011), Connecting the Yakima fold and thrust belt to active faults in the Puget Lowland, Washington, *J. Geophys. Res*., 116, B07105, doi:10.1029/2010JB008091.

Gomberg, J, B. Sherrod, M. Trautman, E. Burns, and D. Snyder (2012), Contemporary Seismicity in and around the Yakima Fold-and-Thrust Belt in Eastern Washington *Bull. Seism. Soc. Am.,* Vol. 102, No. 1, pp. 309–320, doi: 10.1785/0120110065.

Johnson, P. A. (1989), Central Washington seismicity: Evidence for a reactivated buried continental rift and northwest-trending structural zones, *Geophys. Res. Lett*., 16, 1325-1328.

Malone, S. D., G. H. Rothe, and S. W. Smith (1975), Details of microearthquake swarms in the Columbia Basin, Washington, Bull. Seismol. Soc. Am., 65, 855-864.

Rietbrock, A. and F. Waldhauser (2004), A narrowly spaced double-seismic zone in the subducting Nazca plate, *Geophys. Res. Lett.*, 31, L10608, doi:10.1029/2004GL019610.

Schaff, D.P., G.H.R. Bokelmann, W.L. Ellsworth, E. Zanzerkia, F. Waldhauser, and G.C. Beroza (2004), Optimizing correlation techniques for improved earthquake location, Bull. Seism. Soc. Am., 94, 705-721.

Waldhauser, F. and W.L. Ellsworth (2000), A double-difference earthquake location algorithm: Method and application to the northern Hayward fault, *Bull. Seism. Soc. Am.*, 90, 1353-1368.

Waldhauser, F. (2001), HypoDD: A computer program to compute double-difference earthquake locations, *U.S. Geol. Surv. open-file report*, 01-113, Menlo Park, California.

Waldhauser, F. and D.P. Schaff (2008), Large-scale relocation of two decades of Northern California seismicity using cross-correlation and double-difference methods, *J. Geophys. Res*., 113, B08311, doi:10.1029/2007JB005479.

Waldhauser, F. (2009), Near-real-time double-difference event location using long-term seismic archives, with application to Northern California, *Bull. Seism. Soc. Am.*, 99, 2736-2848, doi:10.1785/0120080294.

Wicks, C., W. Thelen, C. Weaver, J. Gomberg, A. Rohay, and P. Bodin (2011), InSAR observations of aseismic slip associated with an earthquake swarm in the Columbia River flood basalts, *J. Geophys. Res.*, 116, B12304, doi:10.1029/2011JB008433.